Steady state plane wave propagation speed in excitable media

Yuri B. Chernyak*
Division of Health Sciences and Technology, Harvard University–Massachusetts Institute of Technology, Cambridge, Massachusetts 02139

(Received 17 June 1996; revised manuscript received 27 March 1997)

With the view to excitation waves in neuromuscular tissue we study the propagation speed c of steady state plane trigger waves as a function of the shape parameters of the nonlinear source function in the reaction diffusion equation (the slow recovery variable is assumed frozen). The nonlinear eigenvalue problem, which yields c as the eigenvalue and the wave profile $u(\xi)$ as the eigenfunction, is reformulated to allow us to construct a variety of exactly solvable models, in particular the waves with profiles having central symmetry about their midpoints. Trigger waves with asymmetric profiles are also considered. The propagation speed c is expressed in terms of the shape parameters of the nonlinear source function $i(u)$. We show that among shape parameters of $i(u)$ there are only three essential ones which control the propagation speed. We derive a general expression for the propagation speed, which has the same simple form as in the well known case with the sawtoothwise $i(u)$ but with one parameter appropriately redefined. We also introduce a simple iterative procedure for solving the nonlinear eigenvalue problem. Finally introducing a new exactly solvable model we show that the effect of noninstantaneous activation on the propagation speed can be reduced to renormalization of one of the steady state model's parameter.
[S1063-651X(97)13808-9]

PACS number(s): 87.22.−q, 82.20.−w

I. INTRODUCTION

Propagation speed of an excitation wave in excitable media was perhaps first estimated in the recently rediscovered [1] early work by Luther [2]. The validity of Luther's expression is limited by the fact that it does not incorporate any nonlinearity parameter responsible for formation of an excitation wave (see Ref. [1]). The nonlinear problem was first introduced for population waves by Fisher [3] and fully solved by Kolmogorov, Petrovskii, and Piskunov (KPP) [4]. In Fisher's and KPP's approach the excitation is realized as an ''ignition'' wave in which a variable u changes from zero to unity. Fisher [3] considered a specific quadratic nonlinear source $f(u)=u(1-u)$ in the reaction diffusion (RD) equation while KPP [4] performed their analysis for an *arbitrary* convex nonlinear source $f(u)$. KPP analyzed global stability of the solutions and showed that the propagation speed is determined by only one parameter of the source function—the slope $f'(1)$ at the final, stable state $u=1$ (the initial state $u=0$ is unstable). An important extension of the KPP results for the nonconvex case can be found in Ref. [5]. It was later discovered that apart from the Fisher-KPP waves some stable faster waves may evolve from some specific initial conditions (see for a review Ref. [6]). Almost simultaneously with Fisher and KPP, Zeldovich and Frank-Kamenetskii [7] considered an ignition wave described by a RD equation with nonconvex source $f(u)$ and using simple physical considerations derived an explicit expression for its speed.

More recent studies in the excitation waves in neuromuscular tissue and autowave chemical reactions revived interest in the propagation speed. The corresponding RD equations incorporate a qualitatively different nonlinear source with three or more nodes, and thus require quite a different approach [8–13]. Besides, after being excited the medium eventually relaxes to the initial state, and this is described by additional ''recovery'' variables obeying extra equations. However, such a complex set of equations can still be reduced to a single RD equation by using the standard approach of singular perturbation theory [8–13]. We shall focus our attention in this paper on electrophysiological excitation waves propagating in neuromuscular tissue and neglect the influence of the slow processes on the back of the wave. Thus, we shall consider *transitional* waves (also referred to as *leading edge* or *trigger* waves) described by a single RD equation (except Sec. VII). Such waves are solutions of a RD equation with a nonlinear source $f(u)=-i(u)$ [$i(u)$ has the meaning of transmembrane current] and therefore all dynamical characteristics of the waves are functionals of $i(u)$. The main aim of this work is to find such a parametrization of the source $i(u)$ that allows one to obtain a general expression for the propagation speed c as a function of the essential shape parameters of $i(u)$. We also demonstrate that the parameters of different source functions can be mapped on each other in such a way that the obtained equation for c holds. In Sec. VII using a specific model we show that the account of activation processes in neuromuscular tissue results only in a minor correction to the propagation speed c and that the shape parameters can be so redefined that the same steady state expression for c remains valid.

II. BASIC EQUATIONS

A. Equations of homogenized syncytium representing neuromuscular tissue

General equations representing neuromuscular tissue as a continuous medium have been only recently derived by Neu

*Corresponding address: Massachusetts Institute of Technology, 77 Massachusetts Avenue, Office E25-330, Cambridge, MA 02139. FAX: (617) 253-3019. Electronic address: yurich@atrium.mit.edu

 © 1997 The American Physical Society

and Krassowska [14] using an appropriate averaging and assuming *periodic* cellular structure. The equations are formulated for the averaged intracellular, extracellular, and transmembrane potentials $\langle\Phi_i\rangle$, $\langle\Phi_e\rangle$, and $U\equiv\langle\Phi^i\rangle-\langle\Phi^e\rangle$, respectively, and in the absence of an external electric field have the form

$$C\partial_t U=L\lambda^i_{\mu\nu}\partial_\mu\partial_\nu\langle\Phi^i\rangle-I(U),$$

$$-C\partial_t U=L\lambda^e_{\mu\nu}\partial_\mu\partial_\nu\langle\Phi_e\rangle+I(U), \tag{1}$$

where C is the surface capacitance of the cellular membrane, L it the cell volume to surface ratio, and $\lambda^i_{\mu\nu}$ and $\lambda^e_{\mu\nu}$ are the effective conductivity tensors arising from averaging, respectively, intra- and extracellular Ohmic currents over the nonisotropic cellular structure [14]. Tacit summation over dummy Greek indices is assumed. The nonlinear source $I(U)$ is the transmembrane current density and is obtained by summing up the membrane I-V characteristics over the cell's surface [14]. A physically consistent theory for the membrane I-V curve can be found in Ref. [15]. Note that Eqs. (1) have been first postulated earlier as the so-called bidomain model of neuromuscular tissue [16,17], a consistent physical interpretation lacking (the term *bipotential model* appears to better represent its content). Remarkably, Eqs. (1) must have broader applicability and hold for nonperiodic and somewhat irregular myocardial tissue as follows from a general mathematical theory of averaging of parabolic operators with almost periodic (or random) rapidly oscillating coefficients [18–20].

We shall consider planar wave configurations with the normal to the plane given by a unit vector $\hat{\mathbf{k}}$, and so the dynamical variables depend on time and the spatial variable $X=\hat{k}_\mu x_\mu$, where $\hat{k}_\mu$ are the direction cosines of $\hat{\mathbf{k}}$ ($\hat{k}_\mu\hat{k}_\mu=1$). In this case Eqs. (1) reduce to a single RD equation of the form

$$\frac{\partial U}{\partial t}=D\,\frac{\partial^2 U}{\partial X^2}-\frac{1}{C}\,I(U),\quad D\equiv\frac{L}{C}\,\frac{\lambda^e\lambda^i}{\lambda^i+\lambda^e}, \tag{2}$$

where $D=D(\hat{\mathbf{k}})$ is the (effective) diffusion coefficient (for the direction $\hat{\mathbf{k}}$) and the invariants λ^e and λ^i are defined as $\lambda^e_{\mu\nu}\hat{k}_\mu\hat{k}_\nu$ and $\lambda^i_{\mu\nu}\hat{k}_\mu\hat{k}_\nu$, respectively. We shall use L as the space scale, $t_0=L^2/D$ as the time scale, $\Delta U=U_{\rm ex}-U_{\rm rest}$ as the potential scale, and $I_0=\lambda_{\rm eff}\Delta U/L$, where $\lambda_{\rm eff}\equiv\lambda^e\lambda^i/(\lambda^e+\lambda^i)$ as the current scale. Note that the velocity unit $L/t_0=\lambda_{\rm eff}/C$ is independent of the spatial scale. In dimensionless form Eq. (2) reduces to

$$\frac{\partial u}{\partial\tau}=\frac{\partial^2 u}{\partial x^2}-i(u), \tag{3}$$

where $\tau=t/t_0$ and $x=X/L$ are dimensionless time and space variables, $u=U/\Delta U$ is dimensionless membrane potential counted off from the resting state, and $i=I/I_0$. A sketch of a typical steady state I-V curve, $i=i(u)$, for myocardium is shown in Fig. 1. In accordance with our definition of u the first and third nodes of $i(u)$ are fixed at $u=0$ and $u=1$. The major *shape parameters* of the curve in Fig. 1 are the end slopes $s_1=i'(0)$ and $s_2=i'(1)$ and the intermediate node u_0 ($0<u_0<1$). A quite remarkable fact is that for neuromuscular tissue the magnitude of the source $i(u)$ in Eq. (3) is always small (our current unit I_0 is large since it is determined by the large electrolytic conductance $\lambda_{\rm eff}$). Using, for example, the popular Luo and Rudy (LR) model [21] (an empirical Hodgkin-Huxley-type model for myocardium) one finds that the peak value of $|i(u)|$ does not exceed 0.015, and moreover both end slopes s_1 and s_2 are also small: $s_1\sim0.54\times10^{-3}$ and $s_2\sim0.034$.

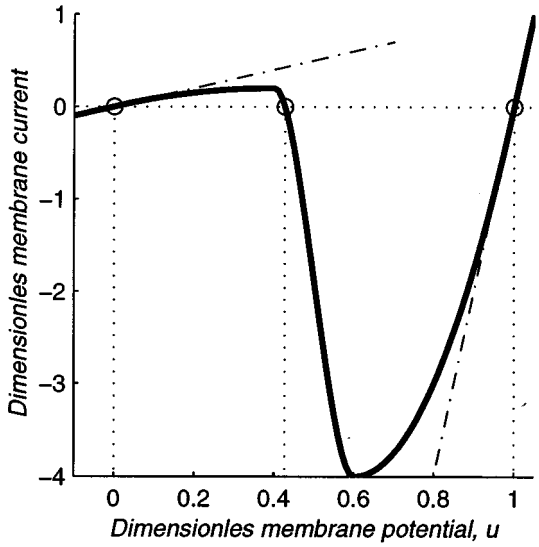

FIG. 1. The sketch of a typical steady state transmembrane current $i(u)$ (arbitrary units) versus membrane potential u. The dash-dotted straight lines $i_1=s_1u$, and $i_2=s_2(u-1)$ show the asymptotics of $i(u)$ for $u\sim0$ and $u\sim1$, respectively. The three nodes of the I-V curve are marked with open circles (the resting state with $u=0$, the unstable transitional value with $u_0\simeq0.4264$ and the excited state with $u=1$). The major shape parameters of the I-V curve are the end slopes $s_1=i'(0)$, $s_2=i'(1)$, and the intermediate node u_0.

B. Nonlinear eigenvalue problem

Considering a plane wave steadily propagating along the x axis from left to right we introduce the usual variable $\xi=x-c\tau$, where c is dimensionless propagation speed, and look for solutions of Eq. (3) depending only on ξ. Setting $u=u(\xi)$ in Eq. (3) immediately gives

$$\frac{d^2u}{d\xi^2}+c\,\frac{du}{d\xi}-i(u)=0. \tag{4}$$

A wave of transitions $u(\xi)$ from the state with $u=0$ at $x=\infty$ to the state with $u=1$ at $x=-\infty$ must satisfy the boundary conditions

$$u(-\infty)=1,\quad u(\infty)=0. \tag{5}$$

The set of equations (4) and (5) is often referred to as a nonlinear eigenvalue problem because as first noted by Zeldovich and Semenov [22] it closely resembles an eigenvalue problem for a linear differential equation of the second order. Problem (4), (5) is usually analyzed using the phase vari-

ables u and $p=du/d\xi$ (often referred to as the KPP variables) in which $d/d\xi \equiv p d/du$, and so Eqs. (4) and (5) reduce to the problem

$$p\,\frac{dp}{du}+cp-i(u)=0, \quad p(0)=0,\ p(1)=0. \tag{6}$$

Since Eqs. (6) involve a first-order equation one can expect that two boundary conditions determine both an integration constant and the propagation speed c. Having found $p(u)$ and recalling that $p=du/d\xi$ and we can find the profile $u=u(\xi)$ in an implicit form as

$$\xi+\text{const}=\int \frac{du}{p(u)}. \tag{7}$$

Since problem (6) involves no parameter, the function $i(u)$ is the only varying element of the problem. This means that c is a functional of the source function $i(u)$. Physically the transmembrane current arises from the activity of a variety of ionic membrane channels, each of which can be independently controlled in experiment, and so the shape of $i(u)$ can be widely varied. For both theoretical and practical applications $i(u)$ can be parametrized, i.e., represented as a fixed function of some parameters, and the dependence of c on such *shape parameters* studied (cf. Refs. [23–27]). The dependence on one particular shape parameter, the magnitude of the nonlinear source, is very simple. One can readily check that problem (6) is invariant under the transformations $i(u)\to\gamma^2 i(u)$, $c\to\gamma c$, and $p\to\gamma p$. This means that the propagation speed c *scales as the square root of the magnitude of* $i(u)$. Because our current unit $I_0=\lambda_{\text{eff}}\Delta U/L$, the dimensional propagation speed is actually proportional to $\lambda_{\text{eff}}/C\sqrt{1/I_0}=\sqrt{\lambda_{\text{eff}}L/\Delta U}/C$. The factor $\sqrt{\lambda_{\text{eff}}}$ includes the entire dependence of the propagation speed on the propagation direction $\hat{\mathbf{k}}$. The above scaling allows us to use in the illustrating calculations of Secs. IV–VI the most convenient for graphical representation normalization of $i(u)$.

III. FACTORIZATION OF THE SOURCE TERM AND TWO MAJOR DISPERSION RELATIONS

The known exactly solvable cases are all designed in a similar fashion: The current $i(u)$ is comprised of two factors, one vanishing at the ends of the interval [0,1] and another one with a node inside the interval, the first factor constituting the solution $p(u)$ of Eqs. (6). For example, for the FitzHugh-Nagumo (FN) equation [13,26] this factor is $\sim u(1-u)$. It suggests that we can view the nonlinear eigenvalue problem (6) as the following *factorization problem:* For a given (source) function $i(u)$ with three nodes at $u=u_1=0$, $u=u_0$, $(0<u_0<1)$, and $u=u_2=1$, find such a constant c $(c\geqslant 0)$ and a continuous function $p(u)$ $[p(u)<0$ for $0<u<1$, $p(0)=p(1)=0]$ that $i(u)$ can be represented as a product

$$i(u)=p(u)j(u), \tag{8}$$

where $j(u)$ is related to $p(u)$ and c as follows:

$$j(u)=p'(u)+c. \tag{9}$$

Since $p(u)\neq 0$ for $0<u<1$ (actually $p<0$) and $i(u)$ has exactly one root on this interval, the second factor $j(u)$ according to Eq. (8) also has exactly one root $u=u_0$ on (0,1). Equation (8) thus represents a factorization of the source $i(u)$ into two factors, one including the nodes at the ends of the interval and another including the intermediate node. It is evident that Eqs. (8) and (9) are equivalent to Eq. (6).

Let us take the derivative of Eq. (8), set $u=0$ or $u=1$, and obtain

$$i'(0)=p'(0)j(0), \quad i'(1)=p'(1)j(1). \tag{10}$$

Introducing the end slopes k_1 and k_2 of the *solution* on the phase plane,

$$k_1=p'(0), \quad k_2=p'(1), \tag{11}$$

one can rewrite Eqs. (10) in the form

$$j(0)=s_1/k_1, \quad j(1)=s_2/k_2, \tag{12}$$

where $s_1=i'(0)$ and $s_2=i'(1)$. The slopes k_1 and k_2 are actually the exponents which determine the asymptotic behavior of the wave front solution $u(\xi)$ as $\xi\to+\infty$ and $\xi\to-\infty$, respectively (the ''foot'' and the ''head'' of the transition wave). Setting $u=0$ in Eq. (9) and using the first relations in Eqs. (11) and (12) we readily obtain

$$k_1^2+ck_1-s_1=0 \quad (k_1<0). \tag{13}$$

This is an asymptotic dispersion relation for the RD equation (3) linearized about the resting state $u=0$ (or $\phi=\phi_r$). [We refer to Eq. (13) as an asymptotic dispersion relation to distinguish it from the dispersion relation arising in the first perturbation order in the two-time theory of nonlinear waves and corresponding to a fundamentally nonlinear periodic process [28,29].] Since the diffusion equation is parabolic, the dispersion relation, which determines the free wave solutions $\exp[ik(x-ct)]$, can be satisfied only for imaginary $k=-ik_1$. The negative slope k_1 $(k_1<0)$ is thus an inverse length constant in the asymptotic solution $u\sim\exp[k_1(x-ct)]$ as $\xi=x-ct\to\infty$. This asymptotic region of exponential growth is often referred in electrophysiology as the ''foot'' of the action potential. Similarly, setting $u=1$ in Eq. (9) and using the second relations in Eqs. (11) and (12) we obtain the second dispersion relation

$$k_2^2+ck_2-s_2=0 \quad (k_2>0), \tag{14}$$

which describes the exponential asymptotics of the transitional wave near the excited state $u=1$. Note that choice of the roots of Eqs. (13) and (14) is specified by the conditions $k_1<0$ and $k_2>0$ [the wave profile $u(\xi)$ is a monotonically decreasing function]. In terms of the phase diagram [10,30,31], dispersion relations (13) and (14) constitute characteristic equations for the saddle points (0,0) and (1,0), respectively, and so the slopes k_1 and k_2 represent *characteristic directions* of the respective saddle points on the (u,p) plane.

Multiplying the differential equation in Eqs. (6) by du and integrating from zero to unity and taking into account the boundary conditions one obtains the well-known identity

$$c=\frac{\int_0^1 i(u)du}{\int_0^1 p(u)du}, \tag{15}$$

which allows one to calculate c after having found the eigenfunction $p(u)$. Using the factorization approach and having found $p(u)$ as $i(u)/p(u)$ one can also find c in a simpler way. Using Eq. (8) one can calculate $j(u)$ and then set in Eq. (9) $u=u_{\min}$ [where $\min\{p(u)\}\equiv p(u_{\min})$] and, because $p'(u_{\min})=0$, obtain $c=j(u_{\min})$. Next, since $p(u)<0$ and $c>0$, Eq. (15) requires that $\int_0^1 i(u)du<0$, which can be written as

$$\int_0^{u_0} i(u)du<-\int_{u_0}^1 i(u)du, \tag{16}$$

where u_0 is the intermediate node of $i(u)$. Thus, Eq. (16) constitutes a condition that the excitation wave propagate in the positive direction of the x axis. Physically, this inequality means that the ''potential energy'' $W=\int_0^u i(u)du$ in the initial state is higher than in the final state, which can be interpreted as the requirement that the transition occurs from a metastable to a stable (ground) state with the lower potential energy $W(1)$ [$W(0)>W(1)$: for details see Ref. [13]].

IV. TRANSITIONAL WAVES WITH CENTRAL SYMMETRY ABOUT THEIR MIDPOINT

A. General consideration

We consider in this section a class of such sources $i(u)$ that they generate solutions $p(u)$ whose graphs on the phase plane are symmetric relative to the vertical $u=1/2$ [$p(u)$ is an even function of $\tilde{u}=u-1/2$]. Such a symmetry of $p(u)$ is necessary and sufficient for the corresponding wave profile $u=u(\xi)$ to have a central symmetry with respect to its midpoint at which $u=1/2$ [for sufficiently smooth $u(\xi)$ the midpoint coincides with the inflection point]. A function $F(u)$ with the domain $0\leqslant u\leqslant 1$ is always representable as a sum of its symmetric and antisymmetric parts $F_+(u)$ and $F_-(u)$, defined as

$$F_+(u)=\frac{F(u)+F(1-u)}{2}, \quad F_-(u)=\frac{F(u)-F(1-u)}{2}. \tag{17}$$

Therefore, if $p(u)$ is symmetric, $p(u)=p_+(u)$, the integral on the right-hand side of Eq. (7) can be written as

$$G(u)=\int_{1/2}^u \frac{du'}{p_+(u')}\equiv\int_{1/2}^u \frac{2du'}{p(u')+p(1-u')}, \tag{18}$$

where the origin of the ξ axis is chosen in the midpoint. One can check that $G(1-u)=-G(u)$, and therefore, the wave profile is determined by the equation $\xi=\tilde{G}(\tilde{u})\equiv G(\frac{1}{2}+\tilde{u})$, where $\tilde{G}(\tilde{u})$ is an odd function of $\tilde{u}$. This can be expressed as $\tilde{u}=\tilde{g}(\xi)$, where $\tilde{g}(\xi)$ is inverse to $\tilde{G}(\tilde{u})$ and hence also an odd function. Therefore, the wave profile has central symmetry relative to the midpoint. The reverse proposition is evident.

A wave with such a symmetry possesses the evident property $p'(0)=-p'(1)$, which, according to Eqs. (11), can be written as

$$k_2=-k_1. \tag{19}$$

This equation and the two dispersion relations (13) and (14) constitute a set of three equations for k_1, k_2, and c, which yield

$$k_2=-k_1=\sqrt{\frac{s_1+s_2}{2}}, \quad c=\frac{s_2-s_1}{\sqrt{2(s_1+s_2)}}. \tag{20}$$

According to Eqs. (20) the direction of propagation of symmetric waves is determined solely by the value of parameter $\lambda=s_1/s_2$, the excitation propagates along the x axis from left to right ($c>0$) when $\lambda<1$, and in the opposite direction otherwise. All symmetric waves have the same propagation speed (20) and the same length scale $1/k_2$ if the end slopes $s_1=i'(0)$ and $s_2=i'(1)$ are, respectively, the same.

The requirement that $p(u)$ be symmetric imposes certain restrictions on $i(u)$. Let us represent $i(u)$ and $p(u)$ as sums of their respective symmetric and antisymmetric parts using Eqs. (17). Since a function and its derivative have opposite parity, we obtain that differential equation (6) is equivalent to the set

$$\begin{aligned} &p'_+p_-+p_+(p'_-+c)=i_+(u),\\ &p_-(p'_-+c)+p'_+p_+=i_-(u). \end{aligned} \tag{21}$$

When p is symmetric, $p=p_+$ and $p_-\equiv 0$, Eqs. (21) reduce to

$$cp(u)=i_+(u), \quad p(u)p'(u)=i_-(u), \tag{22}$$

where $i_+(u)\equiv[i(u)+i(1-u)]/2$ and $i_-(u)\equiv[i(u)-i(1-u)]/2$ are known functions. Note that each of the currents $i_+(u)$ and $i_-(u)$ vanishes at both ends of the segment [0,1]. Equations (22) require that in the symmetric case $i_+(u)$ and $i_-(u)$ be related by

$$i_+(u)\,\frac{di_+(u)}{du}=c^2 i_-(u), \tag{23}$$

where c is the propagation speed given by Eqs. (20). One can also check that, if even and odd parts of $i(u)$ are related by Eq. (23) with an arbitrary chosen constant $c^2>0$, then there is a unique symmetric solution $p=p_+(u)$ related to $i_+(u)$ by the first equality in Eqs. (22) with c given by Eqs. (20). In terms of our factorization problem (8) and (9), condition (23) means that

$$j_+(u)=c, \quad j_-(u)=p'(u)=\frac{1}{c}\,i'_+(u). \tag{24}$$

Thus, for any symmetric function $i_+(u)$, which vanishes at $u=0$ and $u=1$, one can obtain using Eq. (23) the antisymmetric component $i_-(u)$ and the total current $i(u)$ and also find the solutions $p=p_+(u)$ and c.

B. Examples of symmetric solutions

It will be convenient in the following to use renormalized solutions $p_0(u)$ defined by

$$p(u)=k_1p_0(u)\equiv p'(0)p_0(u), \tag{25}$$

and so $p_0(u)>0$ for $0<u<1$ and $p_0'(0)=1$. In the symmetric case we also have $p_0'(1)=-1$. Substituting Eq. (25) into Eqs. (8) and (9) and using Eqs. (20) we obtain

$$i(u)=p_0(u)\left[\frac{s_1+s_2}{2}\,p_0'(u)-\frac{s_2-s_1}{2}\right]. \tag{26}$$

This is a general form of the current corresponding to symmetric solutions and expressed explicitly via the end slopes s_1 and s_2. Let us consider several examples of symmetric exact solutions.

1. Parabolic eigenfunction

Setting $p_0(u)=u(1-u)$ and using Eq. (26) we obtain the FitzHugh-Nagumo (FN) current [13] which has the form of a cubic polynomial:

$$i(u)=u(1-u)[s_1-(s_1+s_2)u]. \tag{27}$$

The intermediate root u_0 is expressed via the end slopes as $u_0=s_1/(s_1+s_2)$. The wave profile $u=u(\xi)$ [we shall hereafter use this simple notation instead of $\tilde{u}=\tilde{g}(\xi)$] can be readily obtained using Eqs. (7) and (25) with $p_0(u)=u(1-u)$. This solution is well known to be given by

$$u(\xi)=\frac{1}{2}\left[1-\tanh\frac{k_2\xi}{2}\right],\quad k_2=\sqrt{\frac{s_1+s_2}{2}}. \tag{28}$$

2. Sinusoidal eigenfunction

A new example of the symmetric exact solution results if one chooses

$$p_0(u)=\frac{1}{\pi}\sin(\pi u). \tag{29}$$

The corresponding current, according to Eq. (26) becomes

$$i(u)=\frac{\sin\pi u}{\pi}\left[\frac{(s_1+s_2)}{2}\cos\pi u-\frac{s_2-s_1}{2}\right]. \tag{30}$$

Note that the intermediate root u_0 of $i(u)$ from Eq. (30) is related to the parameter $\lambda=s_1/s_2$ by $\lambda=\tan^2(\pi u_0/2)$. Simple calculations using Eqs. (7), (25), and (29) give the profile of the transition wave:

$$u(\xi)=\frac{2}{\pi}\arctan[\exp(-k_2\xi)]. \tag{31}$$

Figure 2(A) displays a family of currents (30) and the FN currents (27) for the same two values of of u_0 (which determines the values of parameter $\lambda=s_1/s_2$). In Figs. 2(B) and 2(C) the respective eigenfunctions $p=p(u)$ and the wave profiles $u=u(\xi)$ are plotted. Both the parabolic FN eigenfunctions and their respective wave profiles and the sinusoidal eigenfunctions (29) with their wave profiles (31) have quite similar behavior. All currents are effectively normalized by the condition $c=1$.

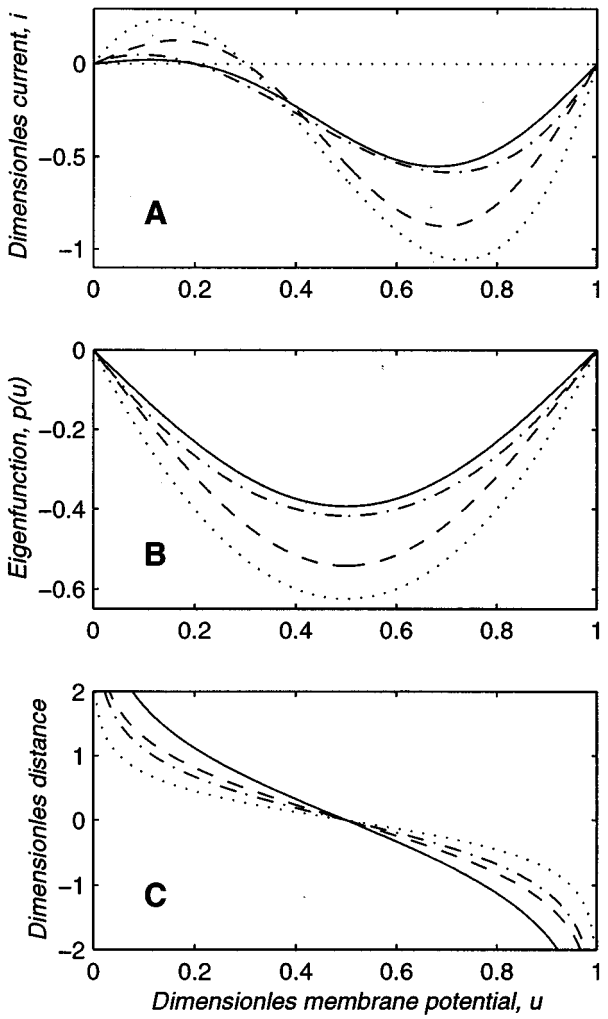

FIG. 2. The triplet of membrane currents (A), eigenfunctions $p(u)\equiv du/d\xi$ (B), and waveprofiles $u(\xi)$ (C) for two different values of u_0 and two different kinds of exact solutions [sinusoidal and parabolic $p(u)$]. The wave profiles in panel (C) propagate ''upward.'' Solid lines ($u_0=0.2$) and dashed lines ($u_0=0.3$) are the currents given by Eq. (30) and $\lambda=\tan^2(\pi u_0/2)$. The FN case with $\lambda=u_0/(1-u_0)$ is shown for the same two values of u_0 by dash-dotted ($u_0=0.2$) and dotted ($u_0=0.3$) lines, respectively. The zero current level is also shown in panel (A) by the dotted line. The requirement $c=1$ for each curve fixes normalization of the current and sets $s_2=2(1+\lambda)/(1-\lambda)^2$ [see second relation in Eq. (20)].

3. Catenary eigenfunction

A more interesting example is generated by $p_0(u)$ shaped as a catenary and depending on a continuous parameter α as follows:

$$p_0(u)=\frac{\cosh\alpha-\cosh\alpha(2u-1)}{2\alpha\,\sinh\alpha}\equiv\frac{\cosh\alpha-\cosh2\alpha\tilde{u}}{2\alpha\,\sinh\alpha}, \tag{32}$$

where the denominator provides the required normalization $p_0'(0)=1$. In the limit $\alpha\to0$, Eq. (32) reduces to the FN expression $u(1-u)$. When $\alpha\gg1$, $p_0(u)$ becomes a tablewise function with the flat top at the height $\sim1/2\alpha$. According to Eq. (26) the current corresponding to Eq. (32) has the form

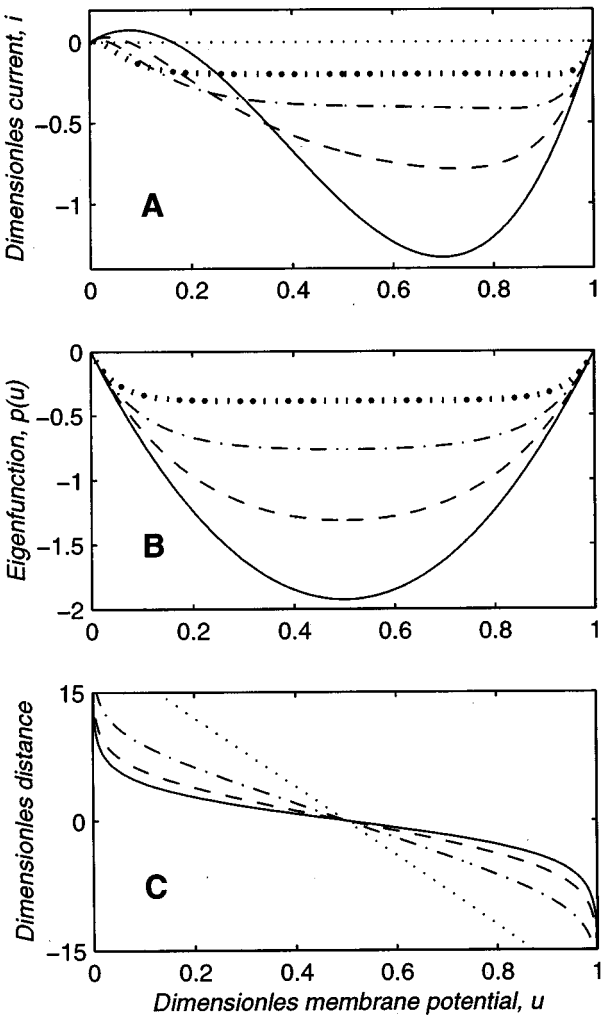

FIG. 3. A triplet of currents (A), eigenfunctions (B), and the symmetric wave profiles (C) given by Eqs. (33), (32), and (34), respectively. Different curves are obtained at the same values of λ and s_2 ($\lambda=0.2$ and $s_2=1$) and $\alpha=2.0$ (solid lines), $\alpha=10$ (dashed lines), $\alpha=5$ (dash-dotted lines), and $\alpha=0.5$ (dotted lines). In panel (A) the horizontal dotted line indicates the zero-current level and all currents normalized by the conditionn $s_2=1$ were multiplied by a factor of 10.

$$i(u)=\frac{\cosh\alpha-\cosh 2\alpha\tilde{u}}{4\alpha\,\sinh^2\alpha}\,[(s_1-s_2)\sinh\alpha - (s_1+s_2)\sinh 2\alpha\tilde{u}]. \tag{33}$$

Figure 3(A) displays a family of such currents (divided by s_2 to scale this parameter out) for a fixed $\lambda\equiv s_1/s_2=0.2$ and $\alpha=0.5,5,10,20$. Although these currents look quite different, the propagation speed has the same value given by Eqs. (20). The scale of the wave width is formally independent of α although the profile of the wave does depend on α. The corresponding eigenfunctions (32) are plotted in Fig. 3(B). Using Eqs. (32), (25), and (7) one obtains the wave profile

$$u(\xi)=\frac{1}{2}-\frac{1}{\alpha}\,\mathrm{atanh}\left(\tanh\frac{\alpha}{2}\tanh\frac{k_2\xi}{2}\right). \tag{34}$$

Note that when $\alpha\to 0$, Eq. (34) reduces to the FN profile (28). Figure 3(C) shows profiles $u(\xi)$ for the respective currents shown in Fig. 3(A) and eigenfunctions shown in Fig. 3(B). One can observe that in the vicinity of the inflection point $\xi=0$ when $\alpha\gg 1$ the eigenfunction becomes approximately constant and the wave profile becomes fairly linear $u(\xi)\approx 1/2-k_2\xi/(4\alpha)$, when $k_2\xi<2\alpha$. When α is large ($\alpha\geqslant 3$) one can visually distinguish three regions of the transition wave, the foot and the head characterized by the same space constant $1/k_2$, and the intermediate linear region with the width $\sim\alpha/k_2$. This example demonstrates that the width of the front and the propagation speed are generally unrelated.

V. ASYMMETRIC CASE

The asymmetric case does not seem to be generally solvable. Nonetheless we shall show in this section that in addition to the end slopes s_1,s_2 one can specify a third parameter, either an asymmetry parameter η, or a growth index ν, or a threshold u_* such that the propagation speed is determined by only these three parameters. We shall also consider some exact solutions which illustrate the interrelationship between different choices and physical interpretations of the third parameter. Any of these exact solutions can be also taken as the first step for the successful approximations considered in Sec. VI.

A. Asymmetry parameter and growth index

At small u, $p(u)\sim k_1u$, and so the nonlinearity of $p(u)$ can be taken into account by a function $\Phi_0(u)$ defined by the equality

$$p(u)=k_1[u-\Phi_0(u)]. \tag{35}$$

Since $p(0)=0$ and $p'(0)=k_1$, we must require that $\Phi_0(0)=0$ and $\Phi_0'(0)=0$. Now taking a derivative of Eq. (35), setting $u=1$, and using Eqs. (11), we obtain $k_2=[1-\Phi_0'(1)]k_1$, which can be written in the form

$$k_2=-\eta k_1, \tag{36}$$

where we have introduced the *asymmetry parameter* $\eta=\Phi_0'(1)-1$. Relation (36) generalizes Eq. (19) to the asymmetric case. Given the values of η and the end slopes s_1,s_2, the propagation speed c can be readily found by solving Eq. (36) simultaneously with the dispersion relations (13) and (14). This yields

$$k_1=-\sqrt{\frac{s_2(1+\eta\lambda)}{\eta(1+\eta)}},\quad k_2=-\eta k_1,$$

$$c=\frac{\sqrt{s_2}(1-\eta^2\lambda)}{\sqrt{\eta(1+\eta)(1+\eta\lambda)}}. \tag{37}$$

When $\eta=1$, Eq. (36) coincides with Eq. (19) while relations (37) reduce to Eqs. (20) for symmetric transitional waves. The excitation condition (16) now reduces to $\eta^2\lambda<1$ or $\eta<1/\sqrt{\lambda}$. The problem of finding the propagation speed c is

thus reduced to finding the asymmetry parameter η. One more step in this direction can be done by introducing a growth index ν defined as

$$\nu = \left. \frac{d \ln \Phi_0(u)}{d \ln u} \right|_{u=0}. \tag{38}$$

The fact that the function Φ_0 has the growth index ν actually means that $\Phi_0(u) = u^{\nu} \Psi_0(u)$, where $\Psi_0(0) \neq 0$. In order to satisfy the condition $\Phi_0'(0) = 0$ we shall consider only $\nu > 1$. Let us impose on $\Psi_0(u)$ the requirements $\Psi_0(1) = 1$ and $\Psi_0'(1) = 0$. Then the conditions $p(1) = 0$, $p'(1) = k_2$ and Eq. (36) are satisfied if we set

$$\eta = \nu - 1. \tag{39}$$

We thus see that the asymmetry parameter η and the propagation speed c *are independent of the function* $\Psi_0(z)$ as long as the conditions $\Psi_0(1) = 1$ and $\Psi_0'(1) = 0$ are satisfied.

B. Exact solutions with asymmetric profiles

1. Power-polynomial current

A simple but nontrivial example of an asymmetric transitional wave arises when one sets $\Psi_0(u) = 1$ or

$$\Phi_0(u) = u^{\eta+1}, \tag{40}$$

with constant $\eta > 0$, which can be treated as a continuously varying parameter. The condition $\eta > 0$ immediately follows from the requirement $\nu > 1$. The FN case corresponds to $\eta = 1$. Some other cases with integer η ($\eta = 2,3$ and $\eta = 4$) were considered in Ref. [32]. The renormalized solution $p_0(u) \equiv p(u)/k_1$ in accordance with Eq. (35) takes the form

$$p_0(u) = u(1 - u^{\eta}), \tag{41}$$

and the current can be obtained using Eqs. (8) and (9) as

$$i(u) = Su(1 - u^{\eta})(u_0^{\eta} - u^{\eta}), \quad S \equiv s_2(1 + \lambda\eta)/\eta, \tag{42}$$

where the intermediate root u_0 is given by

$$u_0 = \left(\frac{\lambda\eta}{1 + \lambda\eta} \right)^{1/\eta}. \tag{43}$$

Equation (37) expresses k_1, k_2, and c via s_1, s_2, and η. The asymmetry parameter η in turn can be represented as a function of the intermediate root u_0 and λ. Solving Eq. (43) for η we obtain $\eta = (1/\lambda)\, r(u_0^{1/\lambda})$ where the function $r(z)$ is defined as a solution to the equation $z = z(r) \equiv [r/(1+r)]^{1/r}$ [i.e., $r(z)$ is an inverse function for $z(r)$]. Both $r(z)$ and $z(r)$ are monotonically growing functions when $r > 0$. Using Eqs. (41), (7), (36), and (25) one can easily obtain the wave profile

$$u(\xi) = (1 + \exp k_2 \xi)^{-\eta}. \tag{44}$$

Figures 4(A)–4(C), respectively, display the corresponding families of the currents $i(u)$, the solutions $p(u)$, and the wave profiles $u(\xi)$.

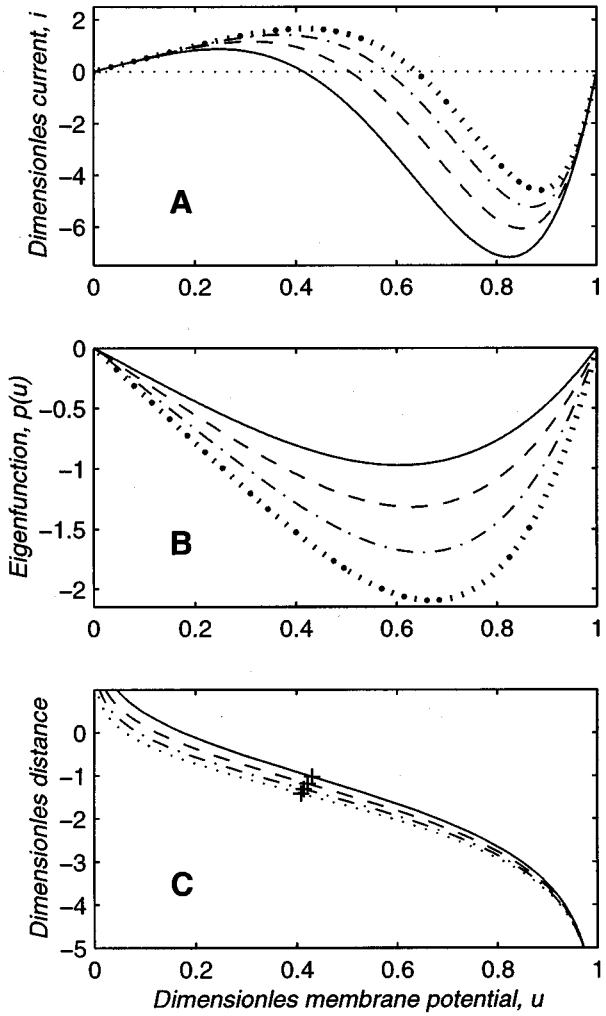

FIG. 4. A triplet of currents (A), eigenfunctions (B), and the (asymmetric) wave profiles (C) for the power-polynomial currents (42) at fixed $\lambda = 0.05$, $s_2 = 1$ [normalization of $i(u)$], and varying η. Solid lines in all three panels correspond to $\eta = 2.5$ and $c = 0.359$; dashed lines, to $\eta = 3$ and $c = 0.31$; dashed-dotted lines, to $\eta = 3.5$ and $c = 0.273$; and dotted lines, to $\eta = 4$ and $c = 0.245$. The inflection points on the wave profiles are marked by asterisks. In panel (A) all currents were multiplied by a factor of 100 and the horizontal dotted line indicates the zero-current level.

2. Piecewise linear discontinuous current

The asymmetry parameter can be expressed solely via an excitation threshold u_* in the following exactly solvable case [26,27] with the sawtooth I-V curve $i = i(u)$ of the form

$$i(u) = \begin{cases} s_1 u & \text{when } u < u_*, \\ s_2(u-1) & \text{when } u \geq u_* \end{cases} \tag{45}$$

[see Fig. 5(A)]. The corresponding continuous eigenfunctions $p(u)$ and the smooth wave profiles $u(\xi)$ are shown in Figs. 5(B) and 6(C), respectively. The current depends on three independent parameters: the end slopes s_1, s_2, and the threshold u_*, the position of the discontinuity of $i(u)$, which plays a role similar to that of the intermediate root u_0 in Eqs. (42). With the view to further generalizations, we shall present below a complete solution of the problem.

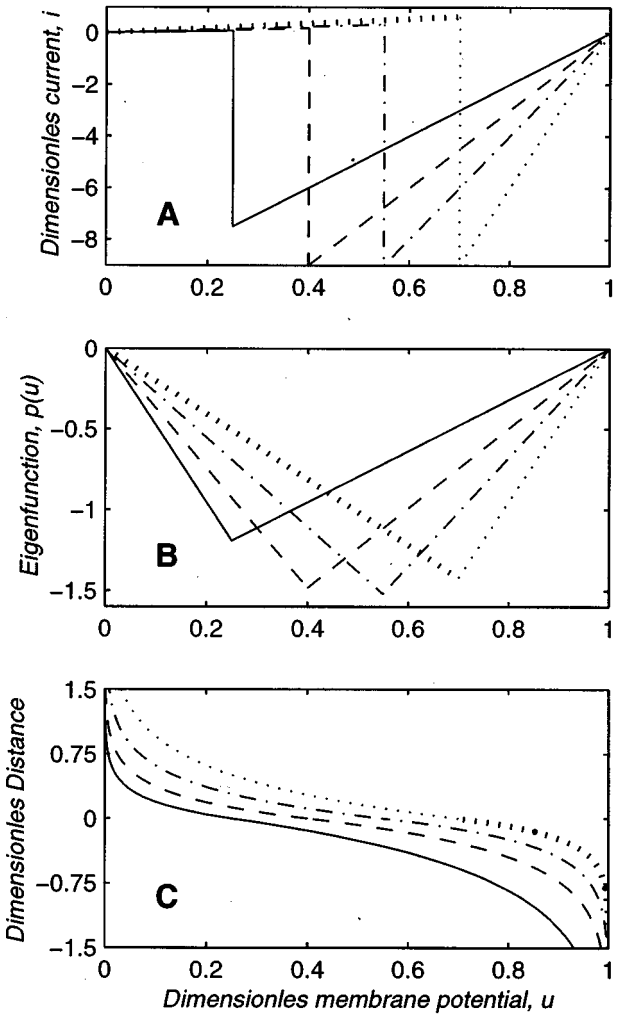

FIG. 5. A triplet of currents (A), eigenfunctions (B), and the (asymmetric) wave profiles (C) for the SZS [27] solvable example. Panels (A), (B), and (C) are described by Eqs. (45), (46), and (50), respectively. Each current is normalized by specifying the value of s_2. For all curves $\lambda=0.03$. Solid lines in all three panels correspond to $s_2=10$ and $c_0=4.70$; dashed lines, to $s_2=15$ and $c=3.59$; dash-dotted lines, to $s_2=20$ and $c=2.55$; and dotted lines, to $s_2=30$ and $c=1.59$. Notice the smoothness of the wave profiles.

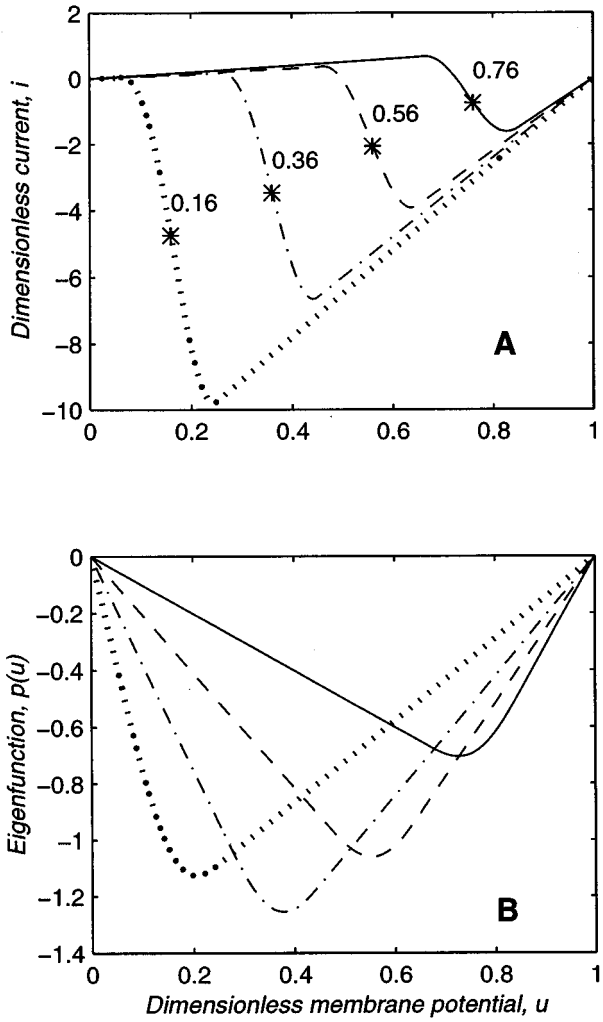

FIG. 6. Continuous membrane currents $i(u)$ (A) and respective eigenfunctions $p(u)$ (B) in the three-piece approximation (51). All curves were calculated at fixed $\nu=2.2$, slightly varied s_1 and s_2, and four positions of the transitional region with the fixed width $\Delta u=0.2$. Solid lines correspond to $s_1=1$, $s_2=10$, the left boundary of the transitional region $u_1=0.651$ (for these parameter values $c\sim 9\times 10^{-17}$); dashed lines correspond to $s_1=0.77$, $s_2=11$, $u_1=0.451$ ($c=1.66$); dash-dotted lines, to $s_1=0.625$, $s_2=12$, $u_1=0.251$ ($c=3.59$); and dotted lines, to $s_1=0.526$, $s_2=13$, $u_1=0.051$ ($c=7.54$). In panel (A) the intermediate points with $u=u_*$ are indicated by asterisks and marked with the u_* values.

It is easy to check that the combination of two linear pieces of the form

$$p(u)=\begin{cases} k_1 u & \text{when } u<u_*, \\ k_2(u-1) & \text{when } u\geqslant u_*, \end{cases} \tag{46}$$

is the exact solution of Eqs. (5) if k_1 and k_2 are the roots of the dispersion relations (13) and (14). The condition that $p(u)$ is continuous at $u=u_*$ reduces to

$$k_2=-\frac{u_*}{1-u_*}\,k_1, \tag{47}$$

which in accordance with Eq. (36) determines the asymmetry parameter η as

$$\eta=\frac{u_*}{1-u_*}. \tag{48}$$

This allows us to use Eqs. (37) and immediately write c as a function of the end slopes s_1, s_2 ($\lambda\equiv s_1/s_2$) and the excitation threshold u_* in the form

$$c=\frac{\sqrt{s_2}[(1-u_*)^2-u_*^2\lambda]}{\sqrt{u_*(1-u_*)[1-u_*(1-\lambda)]}}. \tag{49}$$

The ''foot'' and ''head'' scales k_1, k_2 can also be readily expressed via these parameters using Eqs. (37) and (48). Excitation condition (16), the requirement that $c>0$, now becomes $u_*<1/(1+\sqrt{\lambda})$. Finally, according to Eqs. (7) and (46), the wave profile is a smooth match of the two exponents

$$u(\xi)=\begin{cases}1-(1-u_*)\exp k_2\xi & \text{when } \xi\leqslant 0,\\ u_*\exp k_1\xi & \text{when } \xi\geqslant 0.\end{cases} \quad (50)$$

Next, we shall show that by appropriately redefining the excitation threshold u_* one can extend the above expression (49) to a much more general case with a continuous source current $i(u)$.

3. Continuous current with two linear end regions

A very distinct feature of the neuromuscular tissue is that the ensemble average transmembrane current is fairly linear in each of the two conduction regions corresponding to closed and open sodium channels. A family of currents with such features are shown in Fig. 6(A). The *I-V* curve consists of three regions, the first one in which $u\leqslant u_1$ and $i=s_1\cdot u$, the second, *transitional region* $u_1\leqslant u\leqslant u_2$, and the third region $u>u_2$ in which the current is again linear, $i=s_2\cdot(u-1)$.

In the regions with linear $i(u)$, the eigenfunction $p(u)$ is again linear, $p=k_1\cdot u$ and $p=k_2\cdot(u-1)$, and the entire solution can then be represented as

$$p(u)=\begin{cases}k_1u & \text{when } u\leqslant u_1,\\ k_1[u-\Phi(u-u_1)] & \text{when } u_1\leqslant u\leqslant u_2,\\ k_2(u-1) & \text{when } u_2\leqslant u.\end{cases} \quad (51)$$

Here $\Phi(0)=0$, $\Phi'(0)=0$, which guarantee smooth matching of $p(u)$ and continuity of $i(u)$ at $u=u_1$. By requiring higher derivatives of $\Phi(z)$ to vanish at $z=0$ one can make the matching at $u=u_1$ even more smooth, the smoothness class of $i(u)$ being one unit lower than that of the solution $p(u)$. In order to ensure continuity of $i(u)$ at $u=u_2$ we introduce the *growth index*

$$\nu=\frac{\Phi'(u-u_1)}{\Phi(u-u_1)}\,(u-u_1)\bigg|_{u=u_2}\equiv\frac{d\,\ln\Phi(u)}{d\,\ln u}\bigg|_{u=u_2-u_1}, \quad (52)$$

then set

$$\Phi(u-u_1)=(u-u_1)^{\nu}\Psi(u-u_2), \quad (53)$$

and require $\Psi(0)\neq 0$ and $\Psi'(0)=0$. We shall consider only $\nu>1$ so $\Phi'(0)=0$. We shall show now that the asymmetry parameter η and therefore the propagation speed c *are independent of function* $\Psi(z)$. Using the parameter ν we can define *a weighted medium point* u_* of the transitional region as follows:

$$u_*=\frac{1}{\nu}\,u_1+\left(1-\frac{1}{\nu}\right)u_2. \quad (54)$$

Because the sum of coefficients multiplying u_1 and u_2 in Eq. (54) is unity, the left-hand side of this relation has indeed the form of *a weighted average* of the boundaries u_1 and u_2 of the transitional region (u_1,u_2). Using Eqs. (52)–(54) one can reduce two requirements of smooth matching in Eqs. (51) at $u=u_2$ to Eq. (47) with the threshold value of u_* defined by Eq. (54). Therefore, Eqs. (48) and (49) for η and c also hold true with this redefined value of u_*. Similarly, no new derivation is required to express k_1 and k_2. According to Eq. (54), if one simultaneously shifts the boundaries of the transitional region (u_1,u_2) by δu at fixed ν, the middle point u_* also shifts by δu. This fact in conjunction with expression (49) provides a fairly general answer on the dependence of the propagation speed c on the shape parameters of $i(u)$. Figure 6(B) displays the eigenfunctions (51) in which the function Φ is determined by Eq. (53) with $\Psi=\psi=\text{const}$. That is we set $\Phi(u)\equiv\psi(u-u_1)^{\nu}$ with ψ and ν being constant. Different curves were obtained by shifting the entire transitional region at the fixed value of $\nu=2.2$. The effect of variation of the power ν at a fixed transitional region (u_1,u_2) is exemplified in Fig. 7.

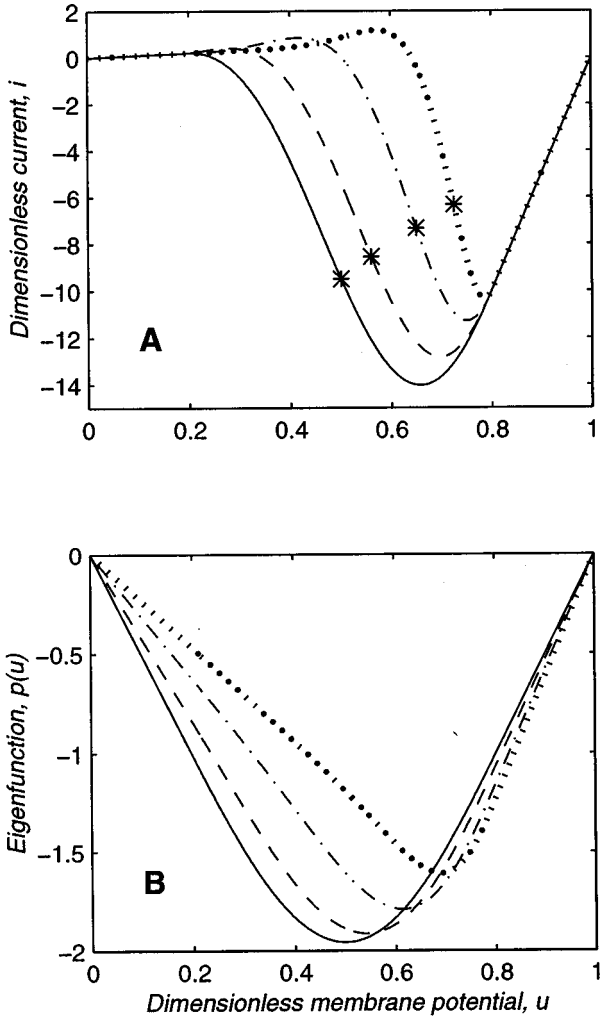

FIG. 7. Continuous membrane currents (A) and respective eigenfunctions (B) in the same three piece approximation as in Fig. 7 but for a fixed transitional region ($u_1=0.2$ $u_2=0.8$), the same end slopes $s_1=1$ and $s_2=50$, and varying power ν. Solid lines correspond to $\nu=2$ ($u_*=0.5$ and $c\sim 4.85$); dashed lines, to $\nu=2.5$ ($u_*=0.56$ and $c\sim 3.97$); dash-dotted lines, to $\nu=4$ ($u_*=0.65$ and $c\sim 2.81$); and dotted lines, to $\nu=8$ ($u_*=0.725$ and $c\sim 1.92$). Asterisks in panel (A) mark the intermediate points with $u=u_*$.

The value of the threshold u_* can be related to the experimentally observable characteristic points of the *I-V* curve such as the intermediate root u_0. Since $p(u)\neq 0$ on the interval $0<u<1$, its inner point u_0 is the root only of the factor $j(u)$ in Eq. (9), which requires one to solve the equation $p'(u_0)+c=0$. The solution is shown in Fig. 8 as a plot of u_* versus u_0 for several values of λ and fixed $\Delta u=0.3$

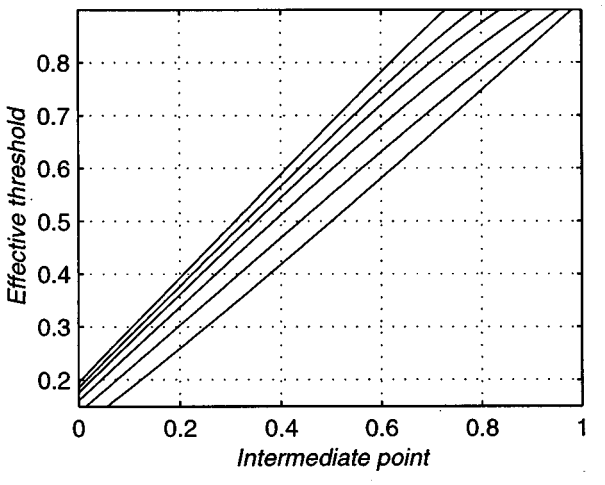

FIG. 8. Dependence of the intermediate point u_* on the intermediate root u_0 at fixed values of $\nu=3$ and $\Delta u=0.3$. The six curves counting from bottom up correspond to $\lambda=0.001$, 0.01, 0.03, 0.09, 0.27, and 0.81, respectively.

and $\nu=3$ [we use Eqs. (51)–(54) with $\Psi=\psi=$const.] The dependence between u_* and u_0 is approximately linear and indicates that u_0 is the first-order estimate for the threshold value u_*.

Returning to a general case of arbitrary function Ψ, one concludes that for given values of u_1 and u_2 the values of k_1, k_2, and c are fully determined by the value of parameter ν and are independent of the (arbitrary) function Ψ in Eq. (53) [as long as $\Psi(0)\neq 0$ and $\Psi'(0)=0$]. If one keeps in mind that in general the end regions can be, however, short, even infinitesimal, the result obtained appears to be fairly important: *Eq. (49) can be considered as a general expression for the propagation speed c via the end slopes s_1,s_2 and the threshold u_*.* An important advantage of the three region representation is that it naturally embodies the three regions of the transitional wave $u=u(\xi)$: the foot with $\xi\to\infty$ and $u\sim\exp k_1\xi$, the middle region which includes the inflection point $u''(\xi_i)=0$, and the head with $\xi\to-\infty$ and $u-1\sim\exp k_2\xi$.

VI. CALCULATIONS FOR AN ARBITRARY SOURCE USING AN ITERATIVE PROCEDURE

We shall introduce in this section a simple algorithm for quickly computing c and $u(\xi)$ for any given source $i(u)$. To simplify our notation we set $\overline{p(u)}=-p(u)$ [so $\overline{p(u)}>0$ on (0,1)], and rewrite the differential equation Eqs. (6) as

$$\frac{d}{du}\left(\frac{\overline{p^2}}{2}\right)=i(u)+c\overline{p(u)}, \tag{55}$$

where $c\geqslant 0$. Now we introduce an important function $I(u)$ defined as

$$I(u)=\int_0^u i(u')du', \tag{56}$$

and write Eq. (55) in the form of the integral relation

$$\overline{p(u)}=\sqrt{2\left[I(u)+c\int_0^u\overline{p(u')}du'\right]}. \tag{57}$$

Relation (57) incorporates the differential equation and the first of the two boundary conditions in Eqs. (6). The second boundary condition $p(1)=0$ requires that

$$I(1)+c\int_0^1\overline{p(u')}du'=0. \tag{58}$$

Note that because $\overline{p(u)}>0$ for $0<u<1$ the integral in Eq. (58) is always positive and we obtain the well-known result that the c vanishes when (and only when) $I(1)=0$. Equations (57) and (58) comprise another formulation of the nonlinear eigenvalue problem and can be considered as a limit of the following sequence of the recurrence relations:

$$c_{k+1}=-\frac{I(1)}{\int_0^1\overline{p_k}(u')du'},$$

$$\overline{p_{k+1}}(u)=\sqrt{2\left[I(u)+c_{k+1}\int_0^u\overline{p_k}(u')du'\right]}. \tag{59}$$

It is evident that if the sequence $\overline{p_k}(u)$ converges at $k\to\infty$ then the limits $\overline{p(u)}=\lim_{k\to\infty}\overline{p_k}(u)$ and $c=\lim_{k\to\infty}c_k$ give the sought after solution of our nonlinear eigenvalue problem. When $I(1)\neq 0$ one can introduce the renormalized quantities $J(u)=I(u)/I(1)$ and $\widetilde{p}_k(u)=\overline{p_k}(u)/\sqrt{-2I(1)}$ and using Eq. (59) obtain

$$\widetilde{p}_{k+1}(u)=\sqrt{\frac{\int_0^u\widetilde{p}_k(u')du'}{\int_0^1\widetilde{p}_k(u')du'}-J(u)}. \tag{60}$$

Because the source term is universally normalized, $J(0)=0$ and $J(1)=1$, the sequence $\widetilde{p}_k(u)$ is actually independent of the value of the integral $I(1)$ and converges to the renormalized solution $\widetilde{p}(u)$ of our eigenvalue problem, $\widetilde{p}(u)\equiv-p(u)/\sqrt{-2I(1)}$. Therefore, Eq. (58) finally yields

$$c=\frac{1}{\sqrt{2}}\frac{\sqrt{-I(1)}}{\int_0^1\widetilde{p}(u)du}, \tag{61}$$

where $\widetilde{p}(u)$ is independent of the details of scaling of $i(u)$. Setting $\widetilde{p}(u)\equiv 1/2$ reduces Eq. (61) to Zeldovich and Frank-Kamenetskii's expression [7] $c=\sqrt{-2I(1)}$ derived for flame propagation (the source without the first node). Our calculations show that for a three-node $i(u)$ it is better to start the iterations with $\widetilde{p}_0(u)\equiv 1$. Setting $\widetilde{p}_0(u)\equiv 1$ in Eq. (60) and using relation (61) we find a convenient first estimate for the propagation speed in the form

$$c\simeq\frac{1}{\sqrt{2}}\frac{\sqrt{-I(1)}}{\int_0^1\sqrt{u-J(u)}du}. \tag{62}$$

Our numerical calculations have shown that Eqs. (59) or (60) and (61) constitute a very convenient, quickly converging, and stable algorithm. In order to avoid the small erroneous imaginary values that may sometimes arise at the very end of the integration interval due to the integration errors it is sufficient to add a small stabilizing positive constant ε_s

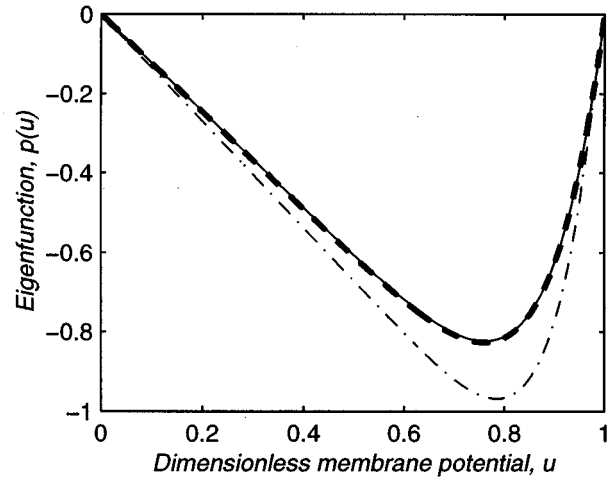

FIG. 9. Iterative solution of solving the nonlinear eigenvalue problem for $i=i(u)$ given by Eq. (42) with $s_1=1$, $s_2=100$, and $\eta=8$. As the zero approximation (dash-dotted line) we took Eq. (51) with $u_1=u_{\max}/2$ and $u_2=(1+u_{\min})/2$ and $\nu=5$, which yields $c_1=0.3586$. The first iteration is shown by the thin solid line and yields $c_1=0.4103$. The second iteration (thick dashed line) is graphically indiscernible from exact solution and gives $c_2=0.4083$. The exact value is $c_1=0.4082$.

under the root in Eq. (59) or (60). The easiest way to calculate such iterative integrals is using the trapezium method, which is precise within $O(\Delta u^2)$. Hence suffices it take $\varepsilon_s \ll \Delta u^2$. In our calculations represented in Fig. 9 we used $\Delta u \sim 1/800$ and took $\varepsilon_s = 10^{-8}$ which stabilized the calculations without affecting the results.

The number of iterations needed to achieve a given precision in $\overline{p(u)}$ depends on the degree of asymmetry of $p(u)$ and, of course, on the initial $\overline{p_0(u)}$. In our numerical experiments the latter dependence was fairly weak. The convergence was the slowest when $p(u)$ was symmetric and was becoming more rapid as the asymmetry parameter was increasing. The worst choice of the zero approximation was $\overline{p_0(u)}=1$ and $c_1=-I(1)$. In most unfavorable cases it could require six or seven iterations to obtain three correct digits in the propagation speed. In most cases it required two to three iterations. The piecewise approximations considered in the previous section comprise a good zero approximation for a variety of the currents we have tried. Figure 9 displays exact and approximate eigenfunctions for the exactly solvable power polynomial current (42) with $s_1=1$, $s_2=100$, and $\eta=8$: The dot-dashed line represents the zero approximation taken in the form (51); the thin solid line results from the first iteration and virtually coincides with the exact solution shown by the bold dashed line. In this and other examples with substantial asymmetry the curves $p=p_k(u)$ become graphically indistinguishable after the second step ($k \geqslant 2$). It usually required one more iteration to reach the same precision when we were starting with a two-piece approximation (45). The method described in this section can also be used in combination with the variational principle introduced in Ref. [33].

VII. MODEL WITH ACTIVATION

We shall consider the effect of noninstantaneous activation on the propagation speed using a generalized sawtooth current model with the threshold u_* varying in time and identified with the control variable w governed by a linear equation. We thus set

$$\frac{\partial u}{\partial t}=\frac{\partial^2 u}{\partial x^2}-i(u,w),$$

$$\varepsilon\,\frac{\partial w}{\partial t}=w_0-w-\delta w\cdot u, \tag{63}$$

where w_0 and δw are positive constants and the current is given by

$$i(u,w)=\begin{cases} s_1 u & \text{if } u<w, \\ s_2(u-1) & \text{if } u\geqslant w. \end{cases} \tag{64}$$

When $\delta w>0$, such a system has two steady states ($u=0$, $w=w_0$) and ($u=1$, $w=w_0-\delta w$). We shall consider a transition wave from the former to the latter state in which $w=w_f=w_0-\delta w$ and $\delta w>0$. Thus, parameter δw has the meaning of the total variation of the control variable w from its initial to the final state. The excitation process is quite simple in terms of the ''potential energy'' $W(u)=\int_0^u i(u')du'$. The ''potential barrier'' between the states with $u=0$ and $u=1$ is $W(w)$ and depends only on w. Even if the initial ''energy'' barrier $W_0 \equiv W(w_0)=s_1 w_0^2/2$ is high, it decreases during activation and finally reaches a lower value of $W_f \equiv W(w_f)=s_1 w_f^2/2$. At the same time the ''energy'' of the final state $W(1)$ becomes lower than that of the initial state $W(0)=0$, and so the system diffuses to the new preferable state.

We shall use the KPP variables and in much the same way as in Sec. II C arrive to the set of equations

$$p\,\frac{dp}{du}+cp=i(u,w),$$

$$\varepsilon c p\,\frac{dw}{du}-w=-w_0+\delta w\cdot u. \tag{65}$$

The function $p(u)$ must satisfy the boundary conditions from Eqs. (6) while the function $w(u)$ must satisfy the condition of nonsingularity: dw/du is bounded at $u=0$ and $u=1$. In terms of variable ξ this condition means that $w(\xi)$ is bounded. In the ''foot'' region $u \leqslant w$ the solution $p=k_1 u$ obtained in Sec. V C for $0 \leqslant u \leqslant u_*$ is still valid. Using the nonsingularity condition and solving the second equation in Eqs. (65) one has

$$w(u)=w_0-\frac{\delta w}{1-\varepsilon c k_1}\,u \quad (\delta w \equiv w_0-w_f), \tag{66}$$

which must hold in the region of the foot of the transition wave where $u \leqslant w$. The excitation occurs when $u=w$, which defines the effective value of the threshold u_*. Therefore, setting $w=u_*$ and $u=u_*$ in Eq. (66) and using Eq. (13) after some calculations one obtains the cubic equation determining the threshold value u_*:

$$\hat{\varepsilon}(1-\lambda)z^3-z^2(1+\delta w-2\hat{\varepsilon}q)$$
$$+z[w_0(1+2\delta w)+\hat{\varepsilon}r]-w_0^2\delta w=0, \quad (67)$$

where $z=w_0-u_*$, $\hat{\varepsilon}=\varepsilon s_2$, $q=1-w_0(1-\lambda)$, and $r=(1-w_0)^2-\lambda w_0^2$. The new smallness parameter $\hat{\varepsilon}=\varepsilon s_2$ is very small for the medium modeling neuromuscular tissue. In the Luo-Rudy model [21], for example, $s_2\sim 3\times 10^{-2}$ and $\varepsilon\sim 10^{-1}$, and so $\hat{\varepsilon}\sim 3\times 10^{-3}$. A solution of Eq. (67) within first order can be obtained readily by setting in Eq. (66) $w=u_*$ and expressing $-ck_1\equiv k_1^2-s_1$ in the zero approximation via $u_*\approx u_*^{(1)}=w_0/(1+\delta w)$. This yields

$$u_*^{(1)}=\frac{w_0}{1+\delta w}\left\{1+\frac{\hat{\varepsilon}\,\delta w}{w_0(1+\delta w)^2}\,[(1-w_f)^2-\lambda w_0^2]\right\}. \quad (68)$$

Further corrections can be found using Eq. (67), if necessary. The fact that the main term in Eq. (68) does not depend on dimensionless activation time scale ε is quite remarkable, since it implies that within the same precision the propagation speed *does not depend on the activation time constant* ε either. Another interesting conclusion from Eq. (68) is that even if ε is of the order of unity the correction due to activation is still small because $\hat{\varepsilon}\sim s_2\ll 1$ (neuromuscular tissue). It is also interesting that in the zero approximation the excitation condition (16) becomes $w_f+\sqrt{\lambda}w_0<1$ and imposes some restriction on the nullclines of the activation equation. This indicates that if λ is not very small and the initial value of the threshold w_0 is sufficiently large the wave would not form and propagate.

VIII. CONCLUSION

As long as the medium can be considered continuous [14,19,20,34] the validity region of our results is mostly limited by the assumptions of fast activation and slow recovery. The former assumption may not be too restrictive because as shown in Sec. VII it can be accounted for by redefining one of the source parameters. An interesting fact generic for neuromuscular tissue is that the dimensionless activation time ε always enters the equations in the combination εc which implies that for slow waves ($c\ll 1$) the activation always occurs fast. The velocity unit for myocardium is fairly large ($c_0\sim 11$ m/s) while the actual propagation speed is about 0.5 m/s. Therefore, excitation waves in myocardium are always slow (the dimensionless speed $c\sim 0.05$) and the parameter $\varepsilon c\ll 1$ even if $\varepsilon\sim 1$. The effect of recovery processes is more complicated particularly because its dimensionless rate ε_1 always appear in the combination ε_1/c. Therefore, the approximation of slow recovery breaks for sufficiently slow waves. It is well known that the recovery processes give birth to the second, slow branch of the dependence of the propagation speed on the threshold, which is broadly believed to correspond to unstable [10] solutions. The slow branch merges with the fast one at a certain minimum speed $c_{\min}$ such that excitation waves with $c<c_{\min}$ do not exist. The value of $c_{\min}$ is the lower bound for the validity region of our results.

Our analysis presented in this paper shows that in the first approximation the propagation speed of excitation waves can be thought of as depending on three major shape parameters of the nonlinear source, the end slopes s_1, s_2 and the threshold u_* or the asymmetry parameter η. We derived a general expression for c in terms of these parameters. Although the asymmetry parameter is in fact a complex functional of $i(u)$, in a number of cases it can be explicitly expressed through the shape parameters of $i(u)$. On the other hand, the parameters η or u_* can be measured in independent experiments. For neuromuscular tissue, for example, the parameter u_* has the meaning of the weighted center of the transitional region of the I-V curve.

An important implication of the exact solutions considered in this paper is that the propagation speed and the width of the wave front are generally independent functionals of the shape of $i(u)$. Only when the source constitutes a one-parameter family [e.g., the Fisher waves [31,35] with $i(u)=-Au(1-u)$ or the waves considered in Ref. [23]], both functionals become different functions of the same single shape parameter and therefore they can be expressed through each other. These solutions also demonstrate that the transition waves may possess more than one characteristic width corresponding to the foot, the head, and the middle of the wave, which may generally vary at fixed c.

ACKNOWLEDGMENTS

I am pleased to use this opportunity to thank Richard J. Cohen and Andrew B. Feldman for stimulating discussions. This work was supported by NASA Grant No. NAGW-3927.

[1] K. Showalter and J. J. Tyson, J. Chem. Educ. **64**, 742 (1987).
[2] R. Luther, Z. Electrochem. **12**, 596 (1906); J. Chem. Educ. **64**, 740 (1987).
[3] R. A. Fisher, Ann. Eugen. **7**, 355, (1937).
[4] A. N. Kolmogorov, I. G. Petrovskii, and N. S. Piskunov, Bull. U. Moscow, Ser. A, No. 6, 1 (1937).
[5] V. E. Gluzberg and Yu. M. L'vovskii, Khim. Fiz. **11**, 1546 (1982).
[6] D. Mollison, J. R. Stat. Soc. B **39**, 283 (1977).
[7] Ya. B. Zeldovich and D. A. Frank-Kamenetskii, in *Chemical Physics and Hydrodynamic, Selected Works of Yakov Borisovich Zeldovich*, edited by J. P. Astriker, G. I. Barenblatt, and R. A. Sunyaev (Princeton University Press, Princeton, NJ, 1992), Vol. I, pp. 262–270.
[8] P. Ortoleva and J. Ross, J. Chem. Phys. **63**, 3398 (1975).
[9] P. Fife, J. Chem. Phys. **64**, 554 (1976).
[10] P. Fife, *Mathematical Aspects of Reacting and Diffusing Systems* (Springer-Verlag, New York, 1979).
[11] J. P. Keener, SIAM (Soc. Ind. Appl. Math.) J. Appl. Math. **39**, 528 (1980).
[12] J. J. Tyson and J. P. Keener, Physica D **32**, 327 (1988).
[13] E. Meron, Phys. Rep. **218**, 1 (1992).
[14] J. C. Neu and W. Krassowska, Crit. Rev. Biomed. Eng. **21**, 137 (1993).

[15] Yu. B. Chernyak, IEEE Trans. Biomed. Eng. **45**, 1145 (1995).
[16] L. Tung, Ph.D. thesis, MIT, Cambridge, MA, 1978.
[17] R. C. Barr and R. Plonsey, Biophys. J. **46**, 1191 (1984).
[18] S. M. Kozlov, Sov. Math Dokl. **18**, 1323 (1977).
[19] S. M. Kozlov, Math. USSR Sbornik **35**, 481 (1979).
[20] S. M. Kozlov, Math. USSR Sbornik, **37**, 167 (1980).
[21] C. Luo and Y. Rudy, Circ. Res. **68**, 501 (1991).
[22] Ya. B. Zeldovich and N. N. Semenov, Sov. Phys. JETP **10**, 1116 (1940).
[23] J. Rinzel and J. B. Keller, Biophys. J. **13**, 1313 (1973).
[24] J. A. Feroe, Biophys. J. **21**, 103 (1978).
[25] L. A. Ostrovsky and V. G. Yakhno, Biofizika **20**, 489 (1975).
[26] A. S. Mikhailov, *Foundation of Synergetics* (Springer-Verlag, New York, 1990).
[27] J. Starobin, Y. I. Zilberter, and C. F. Starmer, Physica D **70**, 321 (1994).
[28] G. B. Whitham, J. Fluid Mech. **22**, 273 (1965).
[29] G. B. Whitham, J. Fluid Mech. **44**, 373 (1970).
[30] K. B. Brushlinskii and Ya. M. Kazhdan, Usp. Matematich. Nauk **18** (2), 3 (1963).
[31] H. P. McKean, Jr., Adv. Math. **4**, 209 (1970).
[32] P. J. Hunter P. A. McNaughton, and D. Noble, Prog. Biophys. Mol. Biol. **30**, 99 (1975).
[33] R. D. Benguria and M. C. Depassier, Phys. Rev. Lett. **77**, 1171 (1996).
[34] J. P. Keener, J. Theor. Biol. **148**, 49 (1991).
[35] J. Canosa, IBM J. Res. Dev. **17**, 307 (1973).